
This is an electronic reprint of the original article.

This reprint may differ from the original in pagination and typographic detail.

Guizani, Chamseddine; Larkiala, Sauli; Moriam, Kaniz; Sawada, Daisuke; Elsayed, Sherif; Rantasalo, Sami; Hummel, Michael; Sixta, Herbert

Air gap spinning of a cellulose solution in [DBNH][OAc] ionic liquid with a novel vertically arranged spinning bath to simulate a closed loop operation in the loncell® process

Published in:

Journal of Applied Polymer Science

DOI:

[10.1002/app.49787](https://doi.org/10.1002/app.49787)

Published: 05/02/2021

Document Version

Publisher's PDF, also known as Version of record

Published under the following license:

CC BY


Please cite the original version:

Guizani, C., Larkiala, S., Moriam, K., Sawada, D., Elsayed, S., Rantasalo, S., Hummel, M., & Sixta, H. (2021). Air gap spinning of a cellulose solution in [DBNH][OAc] ionic liquid with a novel vertically arranged spinning bath to simulate a closed loop operation in the loncell® process. *Journal of Applied Polymer Science*, 138(5), Article 49787. <https://doi.org/10.1002/app.49787>

This material is protected by copyright and other intellectual property rights, and duplication or sale of all or part of any of the repository collections is not permitted, except that material may be duplicated by you for your research use or educational purposes in electronic or print form. You must obtain permission for any other use. Electronic or print copies may not be offered, whether for sale or otherwise to anyone who is not an authorised user.

ARTICLE

Air gap spinning of a cellulose solution in [DBNH][OAc] ionic liquid with a novel vertically arranged spinning bath to simulate a closed loop operation in the Ioncell[®] process

Chamseddine Guizani  | Sauli Larkiala | Kaniz Moriam | Daisuke Sawada | Sherif Elsayed | Sami Rantasalo | Michael Hummel | Herbert Sixta

Department of Bioproducts and Biosystems, Aalto University, Espoo, Finland

Correspondence

Chamseddine Guizani, Department of Bioproducts and Biosystems, Aalto University, P. O. Box 16300, Espoo 00076, Finland.
Email: chamseddine.guizani@aalto.fi

Abstract

A novel, small-volume vertically arranged spin bath was successfully developed for an air gap lyocell-type spinning process. A maximum regeneration bath length with a minimum free volume characterizes the concept of the new spin bath. Using the ionic liquid (IL) 1,5-diazabicyclo[4.3.0]non-5-enium acetate [DBNH][OAc], the spin bath showed very good spinning performances of IL-cellulose dopes at high draw ratios and spinning duration for single filament spinning experiments. Using this new device, it was possible to get a step further in the optimization of the Ioncell[®] process and simulate a process closed loop operation by performing single filament spinning in IL/H₂O mixtures. Good dope spinnability and preserved fibers mechanical properties were achieved in a coagulation bath containing up to 30 wt% IL. It is only at 45 wt% of IL in the bath that the spinnability and fibers mechanical properties started to deteriorate. The fibers fibrillar structure was less pronounced in IL-containing spinning bath in comparison to a pure water bath. However, their crystallinity after washing was preserved regardless of the spinning bath composition. The results presented in this work have a high relevance to the upscaling of emerging IL-based cellulose dissolution and spinning processes.

KEYWORDS

biopolymers, fibers, microscopy, polysaccharides, renewable polymers, X-ray

1 | INTRODUCTION

Ioncell[®] is a new lyocell-type process for the production of man-made cellulosic fibers based on the direct dissolution of a cellulose substrate, preferably a dissolving pulp, in an ionic liquid (IL), air gap spinning of the solution (spinning dope) in a water bath, and a subsequent solvent recovery

step in which the IL, H₂O and impurities generated are separated. The entire process is operated in a closed loop^{1,2}

In industrial-scale continuous processes, cellulose dopes would be regenerated in a coagulation bath containing a mixture of IL and H₂O at the process equilibrium concentration. However, in laboratory tests, the spinning and regeneration of cellulose dopes is mostly performed in

This is an open access article under the terms of the Creative Commons Attribution License, which permits use, distribution and reproduction in any medium, provided the original work is properly cited.

© 2020 The Authors. *Journal of Applied Polymer Science* published by Wiley Periodicals LLC

a pure water bath and not really representative of a continuous process conditions.^{3–6}

The cellulose filaments regeneration kinetic is controlled by the relative diffusive fluxes of the solvent (IL) from the solution into the bath and the nonsolvent (H₂O) from the bath into the gradually forming filament.^{3,7} The diffusive fluxes of the solvent and nonsolvent are proportional to the concentration gradients between the incipient filament and the bath. In addition, the diffusivities of the cation and anion in a H₂O/IL mixture may change with the water mole fraction in the coagulation bath.⁸ These factors make the regeneration process, and possibly the fiber spinning stability (spinnability) dependent on the bath composition.

The change of cellulose regeneration kinetics as a function of the solvent concentration in the coagulation liquid was studied for different cellulose solvent systems, and showed the dependence of the regeneration rate on the coagulation liquid composition^{9–11} Nevertheless, apart from results on diffusivity measurements for H₂O and IL and insights on coagulation mechanisms,^{7,12–15} we could not find data in the literature on cellulose dope spinning in H₂O/IL mixtures, though they are critical for a successful scale up of an IL-based cellulose fiber spinning process.

Acquiring such practical data is often difficult due to the high solvent cost combined to a large spinning bath volume, which makes the spinning tests in H₂O/IL mixtures often impossible or highly expensive.

In this work, we present a novel design of a small-volume vertically arranged spin bath for an air gap lyocell-type spinning process. A maximum regeneration bath length with a minimum free volume characterizes the concept of the new spin bath, in which the amount of IL can be significantly reduced. Using this low volume spinning bath, we conducted single filament spinning experiments in H₂O/IL mixtures with up to 60 wt% of IL in the coagulation liquid. The effects of IL content in the spinning bath on the cellulose dope spinnability and regenerated fibers properties will be discussed accordingly.

2 | MATERIAL AND METHODS

2.1 | Raw materials

2.1.1 | Ionic liquid

1,5-diazabicyclo[4.3.0]non-5-enium acetate ([DBNH][OAc]) was synthesized by protonation of 1,5-diazabicyclo[4.3.0]non-5-ene (DBN) with acetic acid (HOAc). The reagents were both from Fluorochem, UK, with purities higher than 99%. [DBNH][OAc] was

prepared by the slow and controlled addition of an equimolar amount of HOAc to DBN. The mixture was stirred and cooled in the beginning at 25°C to divert the exothermic reaction enthalpy. When approaching equimolar amounts in the mixture, the system was heated at 70°C to avoid the solidification of the IL. The system was kept for another hour at this temperature under mixing to ensure the reaction runs until completion. The water content of the synthesized IL is lower than 0.5 wt%. The stoichiometry of the IL was checked with proton NMR analysis.

2.1.2 | The cellulose pulp

Prehydrolysis-kraft birch dissolving pulp (91.3% cellulose I, mass-average molecular weight, $M_w = 263 \text{ kg mol}^{-1}$, number-average molecular weight, $M_n = 73 \text{ kg mol}^{-1}$ and polydispersity 3.6) was received as air-dried sheets from Stora Enso Enocell mill (Finland), cut into powder form in a Wiley mill (1 mm sieve) and used for the dope preparation.

2.2 | Spinning dope preparation

About 0.5 kg of spinning dope (13 wt% cellulose) was prepared with a vertical kneader system. Air-dried pulp was added to the molten IL while pre-mixing manually with a Teflon spatula. The mixture was then kneaded for 1.5 h at 10 rpm and 80°C in 30–50 mbar vacuum to avoid inclusion of air bubbles. The solution was then press-filtered with a hydraulic press at 2 MPa and 90°C through layered filter mesh (GKD Ymax2, 5 μm nominal, Gebr. Kufferath AG, Germany) to remove the residual undissolved particles.

The spinning dope was then shaped into ~10 g cylindrical pieces (about 10 cm length and 1 cm diameter). Each of the small dope pieces was protected with a plastic film and stored in a closed plastic container inside a cold room at 6°C before conducting the spinning experiments.

To determine the rheological properties of the dope, its viscoelastic behavior was studied using an Anton Paar MCR 300 rheometer with plate-plate geometry (25 mm plate diameter, 1 mm gap size) according to the procedure described in.¹⁶ From the rheological data, and prior observation on the spinning stability zone of similar dopes, we could determine the target spinning temperature window (73–79°C), corresponding to a zero shear viscosity about 30,000 Pa.s and an angular frequency at the cross over point of 1 Hz.¹⁶ More details about the rheological data are given in Figure S1 in the electronic supporting information (ESI).

2.3 | The gram-scale spinning unit

2.3.1 | Background

A gram-scale, monofilament spinning device used in our laboratory experienced some limitations regarding spinning behavior and comparability with the larger multifilament spinning systems.^{17,18} The existing coagulation bath was identified as the main cause of the impaired spinning behavior: uncontrolled temperature and no fluid circulation, leading to poor mass transfer conditions. In addition, this coagulation bath had a volume of 24 L, which is already quite high for conducting spinning experiments with significant amount of IL in the coagulation liquid.

In order to fast-screen spinning parameters, like IL type and concentration in the bath, we needed to revisit the design of the gram-scale spinning unit and design a novel coagulation bath in order to meet good performances at reasonable costs and operating time. New designs presented in the literature do not meet the full requirements we needed. For instance, Klar et al.¹⁹ developed the so called channel spinning method in which they vary the angle of the inclined channel and the flow rate of ethanol to adjust the external force applied to the yarn and the extent of drawing. However, high draw ratios (DRs) would be difficult to achieve using only the drag force caused by the flowing liquid. Turbulences in the spinning channel would be unavoidable beyond a certain flowrate limit, and will be detrimental to the spinning operation.

2.3.2 | Design of the new coagulation bath

One of our main design goals was to minimize the volume of the spin bath in order to limit the amounts of IL in the coagulation liquid, while maintaining a long enough residence time for a complete coagulation of the incipient filament.

Reducing the volume of a spin bath is not a straightforward task, as it is limited by factors related to the dope regeneration length (depth of the bath), take-up angle (length of the bath) and operator manual access to the filament in order to start the filament take-up at a defined DR (width of the bath).

Preliminary calculations showed that a classical rectangular or trapezoidal bath geometries does not allow reducing extensively the volume down to a five liters target we set. We considered then a design option based on a falling-jet reactor as described in.²⁰ For this type of design, the requirements were:

- A sufficiently long water column above the jet exit to assure regeneration.
- A wide enough jet exit to allow the filament(s) to pass through.
- A moderate water stream at the top surface to minimize turbulences.
- A constant water level to ensure a constant air gap.
- A moderate water jet velocity at the exit to avoid excessive drag on the filament.

The reader can immediately notice how conflicting those requirements turn out to be. Increasing the regeneration length leads to a higher water jet velocity following Torricelli's law: $v_{\text{jet}} = \sqrt{2g\Delta h}$, and to a higher drag force (F_{Dg}) on the filament, which scales with the jet velocity. Here, v_{jet} is the water jet velocity, g is the gravitational acceleration and Δh is the length of the water column above the jet exit point.

Increasing the regeneration length means also circulating a higher volumetric water flow ($\dot{V}_{\text{H}_2\text{O}}$) in the coagulation bath, which will also increase the turbulence at the top of the bath, quantified by an increase of the Reynolds number (Re). In a similar way, increasing the exit jet diameter (d_{jet}) leads to a higher volumetric water flow circulation ($\dot{V}_{\text{H}_2\text{O}} \propto d_{\text{jet}}^2$), which increases the turbulence at the top part of the reactor ($\text{Re} \propto d_{\text{jet}}^2$).

A possible way to harmonize between those conflicting requirements, namely a long enough regeneration length, a wide enough jet exit diameter, a laminar flow at the top part and a moderate jet velocity at the exit, is to reduce the hydrostatic pressure at the jet exit point by lifting it to a higher vertical position. This could be achieved with the new monofilament spinning unit design illustrated in Figure 1. With this new design, the height difference Δh between the top surface of the water in the coagulation bath and the tube exit is only of few centimeters (2–3 cm), while the regeneration length is about 1.9 m.

The spinning cylinder is located at the top right of the computer-aided design (CAD) design shown in Figure 1(a). The dope is extruded from the spinning cylinder (1) into the coagulation bath through a spinneret having a single 100 μm diameter hole.

The coagulation bath is located just below the spinning cylinder (1) and fixed on a metallic frame, which vertical position can be controlled by an electrical motor (2). The coagulation bath consists of four parts, which can be easily connected and dismantled for cleaning:

- An upper part (3) having two connections (diameter = 10 mm) for the fluid inlet (bottom right) and overflow (top left). Two concentric cylinders (diameters of 60 and 135 mm) form this upper part. The

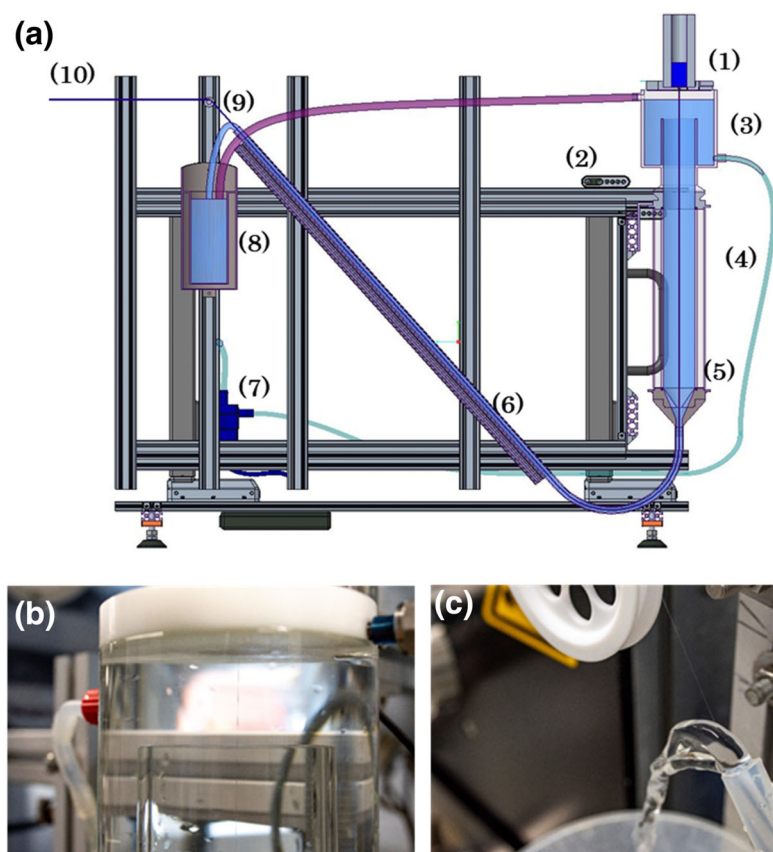


FIGURE 1 (a) CAD of the new experimental set up for single filament spinning; (b) photograph of the top of the spin bath showing the filament during spinning and the still water surface; (c) photograph showing the water jet and the filament collected by the operator at the exit tube during a spinning experiment [Color figure can be viewed at wileyonlinelibrary.com]

annular zone between the outer and inner cylinder helps reducing the fluid velocity and turbulence. The annular space provides a greater area for the fluid to flow in and reduces its velocity close to the filament penetrating the bath. Part of the fluid flows downward and the other part through the overflow in order to maintain a constant fluid level inside the bath.

- A middle cylindrical part (4) with a diameter of 60 mm and a length of 460 mm.
- A bottom conical part (5) ending with a diameter of 16 mm.
- An exit tube (6) with a diameter of 16 mm, directed upward at a 50° angle and having a length of about 1250 mm.

A centrifugal pump (7) ensures a closed-loop circulation of the coagulation liquid (H₂O or IL/ H₂O mixtures) from the spin bath (exit tube and overflow) into a water-cooled double-jacketed metallic reservoir (8). The 5°C cold water circulating in the reservoir double jacket allows to cool down the coagulation bath liquid down to a temperature in the range of 9–11°C.

A rotameter allows adjusting the flow rate and the level of the coagulation liquid. Using a total water flow rate of 1.9 L/min, nearly 68% of the flow returns into the container through the overflow, and 32% through the exit

tube (9). With this new design, the total volume of the liquid is less than 5 L.

When the filament enters the coagulation bath, several forces act on it: the gravity force, the buoyancy force, the viscous friction and the liquid drag force. The resultant force is directed downward, without being too high to induce a visible filament stretch. The continuous diameter reduction in the conical part allows a smooth and continuous increase of the coagulation liquid velocity and drag force. Once the filament arrives at the bottom of the conical part, the coagulation liquid velocity is high enough to induce a drag force that pushes the filament in the upward direction inside the 50° inclined tube, until it reaches the jet exit. The operator simply takes it at the exit of the jet (10) and can start the take up operation.

2.4 | Spinning experiments

Prior to spinning, the metallic cylinder was heated to 75°C, loaded with a piece of solidified dope (~10 g) and left for at least 2 h until the dope melts. Filament spinning was done using a single hole spinneret (Enka Teknica, Germany) having a diameter (D) of 100 μm . The extrusion velocity v_{ext} was held constant at 0.015 $\text{cm}^{21}/\text{min}$ (1.9 m/min). By adjusting to the right take-up

velocity v_{tip} , the draw ratio $R = \frac{v_{\text{tip}}}{v_{\text{ext}}}$, was increased constantly through the experiment in order to determine the maximal achievable DR. The dope spinnability is quantified through the maximal achievable DR and the spinning duration. The higher the DR and the spinning time, the better is the spinnability. We estimate that the dope spinnability is good at a defined DR if the spinning time exceeds 5 min.

2.4.1 | Suitability of the novel coagulation bath for single filament spinning

The suitability of the new bath for a single filament spinning was first and extensively investigated in a pure water over a wide range of DRs (from 1 to 13) and using three different spinnerets with capillary length to diameter ratio (L/D) of 0.2, 1, and 2. The bath temperature was maintained in the range of 9–11°C.

2.4.2 | Spinning in IL/H₂O mixtures

After the initial optimization tests in pure water, dope spinning in IL/ H₂O mixtures was tested for IL concentrations in the bath of 0, 15, 30, 45, and 60 wt%. The spinning experiments were performed using a spinneret with L/D = 2. Mixtures of IL and H₂O were prepared by mixing IL and water in the defined mass proportions. The total mass of the mixture was five kilograms. Using an electronic scale (precision of 0.1 g), water was added to the IL progressively while mixing until reaching the target mass. The mixture was then poured in the coagulation bath, put into circulation and cooled progressively until it attained the steady state temperature (9–11°C).

2.5 | Fibers properties

2.5.1 | Fiber elongation, tenacity, and titer

Fiber elongation, tenacity and titer were measured using a Favigraph tensile tester (Textechno H. Stein GmbH & Cpo, Germany), with at least 0.6 cN/tex pretension in the conditioned state (temperature of $20 \pm 2^\circ\text{C}$ and relative humidity of $65 \pm 2\%$). Average values from 20 individual fibers are calculated. The gauge length was 20 mm and the testing speed was 20 mm/min. The pretension weights were 100–500 mg and maximum force of the cell load was 20 cN or 100 cN.

2.5.2 | Wide-angle X-ray diffraction and small angle X-ray scattering

Spun fibers for X-ray diffraction (XRD) were thoroughly washed by water before the experiment. XRD data were collected using SmartLab (RIGAKU) instrument operated at 45 mA and 200 kV ($\lambda = 1.5418 \text{ \AA}$). Ioncell® fibers were cut into small pieces and tightly packed in a Mylar film (Dupont). The samples were fixed on a sample holder with a transmission geometry. Powder diffraction data were collected in the continuous line scan mode with $\theta/2\theta$ geometry from 5 to $60^\circ 2\theta$. Data collection were performed in two different geometry by setting χ angle of sample holder at 0° and 90° in order to average little effect of preferential orientation of fibrous samples. Mylar diffraction profiles without sample was collected under the same experimental condition, and it was subtracted from intensity profiles of samples. The subtracted data were smoothed using Savitzky–Golay²² filter with a window size of 29 and a polynomial order of one. The smoothed data were corrected for inelastic scattering.

The background profile ($I_{\text{bkg}}[\theta]$) was estimated using a smoothing method^{23,24} applying Savitzky–Golay filter from 8 to $55^\circ 2\theta$ for each diffraction profile. Window size and polynomial order for the Savitzky–Golay filter were set to 201 (corresponding to 4° by 2θ) and 1, respectively. Iteration for the background estimation was repeated 50 times until the iteration does not reduce the background area significantly. Then the crystallinity index (CI) was estimated using the ratio of the area of total intensity and of the above estimated background intensity from 9 to $50^\circ 2\theta$:

$$\text{CI} = 100 * \frac{\int I(\theta) d\theta - \int I_{\text{bkg}}(\theta) d\theta}{\int I(\theta) d\theta} \quad (1)$$

The background corrected profiles in the range from 8 to $26^\circ 2\theta$ were fitted with four pseudo-Voigt functions for 1–1 0, 1 1 0, and 0 2 0 equatorial diffraction peaks, and a diffraction peak for meridian 0 0 2 peak. Latter meridian peak was added because a visible shoulder was present at $17.2^\circ 2\theta$ probably due to the preferential orientation originated from the fibrous morphology of the samples. A software lmfitt²⁵ was used for the fitting. Scherrer equation was used to estimate the crystal widths (CW_{hkl}) of equatorial lattice of cellulose II as follows:

$$\text{CW}_{\text{hkl}} = \frac{K \lambda}{\beta_{\text{hkl}} \cos \theta} \quad (2)$$

where $K = 0.90$ is shape factor, λ is the X-ray wavelength, β_{hkl} is the full width at half maximum of the diffraction

peak in radians and θ is the diffraction angle of the peak. Due to the significant overlap of diffraction peaks, the crystal widths were reported by the average from three equatorial diffraction peaks.

Synchrotron X-ray data were collected at beamline D2AM at ESRF (Grenoble, France). The fiber samples were mounted on multi-position sample holder. Simultaneous wide- and small-angle scattering patterns (WAXS/SAXS) were collected in the transmission mode using flat 2D “WOS” (WOS stands for WAXS Open for SAXS detector) detector for wide-angle and 2D detector “XPAD-D5” for small angle (imXPAD, France). X-ray energy was set to 18 keV ($\lambda = 0.688801 \text{ \AA}$). Sample to detector distance was calibrated using Cr_2O_3 powder for WAXS and silver behenate for SAXS.

Both WAXS and SAXS data were processed using pyFAI,²⁶ a python library for azimuthal integration of diffraction data. For WAXS, raw 2D images were processed correcting for the detector distortion, normalizing for the incident beam intensity and subtracting scattering contribution from air. Herman's orientation parameter between cylindrical longitudinal direction and the crystallographic c-axis of unit cell was estimated from the azimuthal profile of 0 2 0 diffraction peak assuming cylindrical symmetry along the fiber as previously described.²⁷ Crystallinity was calculated in the same way as previous description for Smartlab instrument except for the use of azimuthal integrated intensity profile from the equatorial diffraction. Due to the detector limitation, background intensity was estimated for the range between 7 and 32° by $\text{CuK}\alpha$ 2 θ , and window size for the Savitzky–Golay filter were set to 31 (corresponding to 4° by $\text{CuK}\alpha$ 2 θ). Crystallinity was estimated for the range between 9 and 32° by $\text{CuK}\alpha$ 2 θ .

SAXS data were processed correcting for the detector distortion, normalizing for the incident beam intensity and subtracting scattering contribution from air. Then Herman's parameter was estimated using the same method as WAXS, but from the equatorial streak at $q = 0.01 \text{ (\AA}^{-1}\text{)}$.

2.5.3 | Fibers morphology

Scanning electron microscopy (SEM) imaging of the Ioncell fibers were taken with a Zeiss Sigma VP electron microscope with a 1.2–1.5 kV operating voltage and a secondary electron detector (topography mode). The fibers were cryo-fractured by dipping a fiber bundle into liquid nitrogen, fracturing it and gluing it vertically onto the conductive support. The samples were sputter-coated with a gold layer (90 s with a 20 mA current which forms ~9 nm layer of gold on the surface) to enhance the electric conductivity and avoid surface charging phenomenon.

3 | RESULTS AND DISCUSSION

3.1 | Suitability of the novel bath for single filament spinning

3.1.1 | Dope spinnability in a pure water bath

Dope spinning trials in pure water were performed in order to assess the spinnability performance using the new coagulation bath. Spinnerets with three different aspect ratios (L/D of 0.2, 1, and 2) were used to evaluate the spinnability and fibers properties. The spinnability results (time vs. DR) for the different spinneret aspect ratios are shown in Figure 2 in the ESI.

The main findings are:

- Dope spinning at a DR = 10 or below was successful regardless of the spinneret aspect ratio.
- The spinnability improves when increasing the spinneret aspect ratio.
- Continuous spinning for a duration as high as 25 min was possible at a DR of 12 with an L/D = 2.

All in all, those results indicate that with this new experimental device, better spinning performances are achieved in comparison to previously reported results in^{17,18} using the old system.

It is worth noting also that when the filament breaks, the breakage occurred mainly at the top part of the reactor close to the coagulation bath surface. It was very scarce that breakages occurred at the bottom-curved part of the exit of the tube. This location was initially thought to be the most critical part, due to possible high frictions between the filament and the silicon tube surface. This was not the case. One reason could be that the water inside the exit tube works as a lubricant and reduces the friction between the filament and the curved silicon tube wall.

3.1.2 | Fibers properties

Fiber tenacity, elongation, and titer

The tenacity, elongation and linear density of the fibers obtained in a water coagulation bath with different L/D ratios are shown in Figure 2. The evolution of the titer with the DR is almost the same regardless of the L/D ratio in the spinneret. The titer variation with the DR is well represented by an inverse proportion relationship. A slightly better fitting could be obtained when allowing the power coefficient to vary around minus one. The nonlinear least square fitting gives in this case a constant

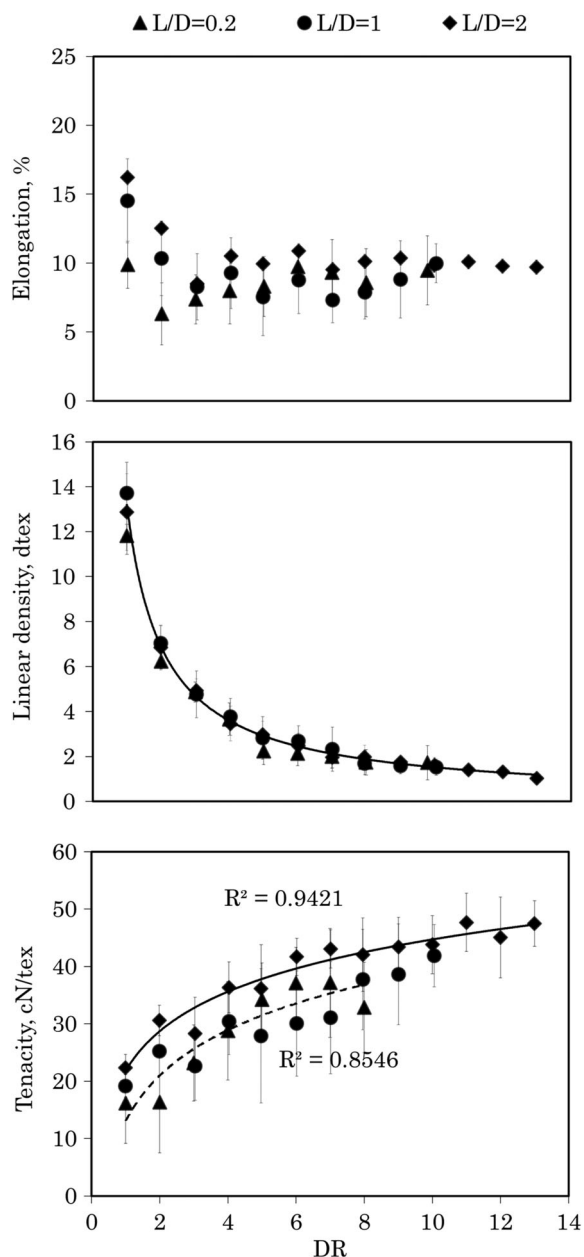


FIGURE 2 Fiber properties as a function of the DR for the different L/D in the spinneret capillary. Spinning conditions: $v_{ext} = 1.9$ m/min, bath temperature = 10°C. DRs, draw ratios

factor and a power coefficient respectively of 13.175 and -0.938 . Those values are slightly different from the ones previously determined: 13.88 and -1.236 .³

As expected, the tenacity increases with the DR. The increase in tenacity levels-off beyond DR 6. Although the statistical significance might be an issue due to relatively large errors bars, there is a trend towards a tenacity improvement when increasing the spinneret L/D ratio. A mathematical fitting of the experimental data with a logarithmic function (R^2 of 0.94 and 0.87 respectively for L/D of 0.2 and 2) was added to the plot to help the reader

visualizing the differences. Regardless of the L/D ratio in the spinneret, the fiber elongation decreases markedly between DR 1 and 3, and then stabilizes beyond DR 6. Here again, the elongation values are improved when increasing the L/D, especially for low DR values. The elongation values for the highest L/D are constantly above the ones obtained at low L/D. Nevertheless, the L/D effect is less marked beyond DR 4.

As pointed out previously, the improved fibers properties at higher L/D might be due to a higher shear inside the longer capillary resulting into a higher cellulose chains orientation, which translates to better mechanical properties of the resulting fibers.¹⁷ Fiber elongation and tenacity can be combined into a toughness value representing their product. The fiber toughness was calculated and compared for the three aspect ratios. The results given in Figure S3 in the ESI and show clearly that increasing the L/D in the spinneret leads to stronger fibers. Altogether, those observations imply that the spinneret L/D affects directly the fiber properties and should be considered in the process optimization stage.

Crystalline orientation, voids orientation, and crystallinity

Crystalline orientation, voids orientation and crystallinity increase moderately at DRs between 4 and 12 (see Figure S4 in the ESI). The three parameters correlate with the tenacity. Slightly steeper increase of crystalline orientation at DR between 0.5 and 4 is probably a reason for the tenacity increase below DR 6 before the leveling off. As compared to a previous report from standard spinning unit with L/D 0.2,²⁸ crystalline orientation parameter increased sharply at DR between 1 and 11.

3.2 | Discussion about the spinning efficiency using the novel spinning bath

The novel spinning bath showed very good spinning performances in single filament spinning. We believe that those performances stem from the good hydrodynamics as well as from the relatively long filament residence time inside the bath. We discuss here those two issues with the aid of numerical simulation.

3.2.1 | Hydrodynamics in the spin bath

During spinning experiments, the water surface at the top of the bath was free of turbulences and almost still (see Figure 1(b)). At the bottom of the bath conical part, the water velocity was significantly higher, which generated a high-enough drag force to push the filament

towards the exit, so that the operator can easily recover it and start the take-up operation (see Figure 1(b)).

In order to have more insight on the fluid flow dynamics, the water flow inside the new coagulation bath was simulated using COMSOL Multiphysics, by solving numerically the continuity and the Navier–Stokes equations in the bath geometry, considering:

- A steady state, 3-D model.
- An incompressible flow in a laminar regime (justified by the low enough Reynolds and Mach numbers).

The continuity equation then reads:

$$\rho \nabla \cdot \mathbf{v} = 0. \quad (3)$$

The Navier–Stokes equation reads:

$$\rho (\mathbf{v} \cdot \nabla) \mathbf{v} = \nabla \cdot (-p \mathbf{I} + \mathbf{K}) + \rho \mathbf{g}. \quad (4)$$

With \mathbf{K} corresponding to:

$$\mathbf{K} = \mu (\nabla \mathbf{v} + [\nabla \mathbf{v}]^T). \quad (5)$$

Those equations are at the core of fluid flow modeling. Solving them, for a set of boundary conditions (such as inlets, outlets, and walls), predicts the fluid velocity and its pressure in a given geometry.

The boundary conditions were defined as:

- A constant volumetric flow of 1.9 L/min at the inlet (upper part).
- A constant pressure at the outlet (overflow and exit tube).
- A zero-slip velocity at the bath walls and at the bath top surface.

A predefined physics-controlled mesh (fine mesh) was used to split the bath geometry into 21,899 domain elements, 4624 boundary elements, and 955 edge elements.

Simulation results showing the water velocity magnitude and field are depicted in Figure 3. From the different 2-D sections shown in this figure, the reader can see how the fluid velocity drops when flowing from the inlet into the annular space of the upper part providing low turbulences at the surface of the coagulation bath, and increases afterwards close to the exit of the conical bottom part providing enough drag to drive the filament towards the exit tube. The average Reynolds number was around 22 in the top part annular space and increased to around 950 at the level of bottom conical part. The simulation also predicts that around 70% of the total flow goes

through the overflow exit, and 30% goes through the exit tube. Those values are quite in line with what we measured experimentally with deviations lower than 4%.

3.2.2 | The filament residence time inside the spin bath

In order to remove the IL and regenerate the cellulose into filament, the residence time of the incipient filament inside the bath must be long enough to allow the diffusion of the IL in the bath and water inside the filament. This residence time can be translated into a regeneration length by simply multiplying it by the take up velocity.

In this regard, it is interesting to compare the length needed for regeneration with the one provided in the new set-up. To do so, we simulated the diffusion of IL and water during the spinning in this novel coagulation bath, with the aim to estimate the residual IL concentration in the filament at the exit point.

In this simulation, we considered the case of spinning at a DR 10 with an extrusion velocity of 1.9 m/min, which was experimentally successful regardless of the spinneret aspect ratio. We assumed that all the stretch occurs in the air gap. The conservation of mass leads to a wet incipient filament radius of 15.8 μm when entering the coagulation bath. The diffusion coefficient of [DBNH][OAc] and H_2O were previously determined in³ and used in the present simulation.

The diffusion of IL and H_2O is modeled with a time dependent, 1-D axisymmetric model using the software COMSOL Multiphysics.

The diffusion equation according to Fick's second law reads:

$$\frac{dC_i}{dt} = -\nabla \cdot (-D_i \nabla C_i), i = \text{H}_2\text{O}, \text{IL}. \quad (6)$$

The initial concentrations for water and IL concentrations in the incipient filament are:

$$C_{\text{H}_2\text{O}}(r, 0) = 0. \quad (7)$$

$$C_{\text{IL}}(r, 0) = C_{\text{IL}0}. \quad (8)$$

The boundary conditions are:

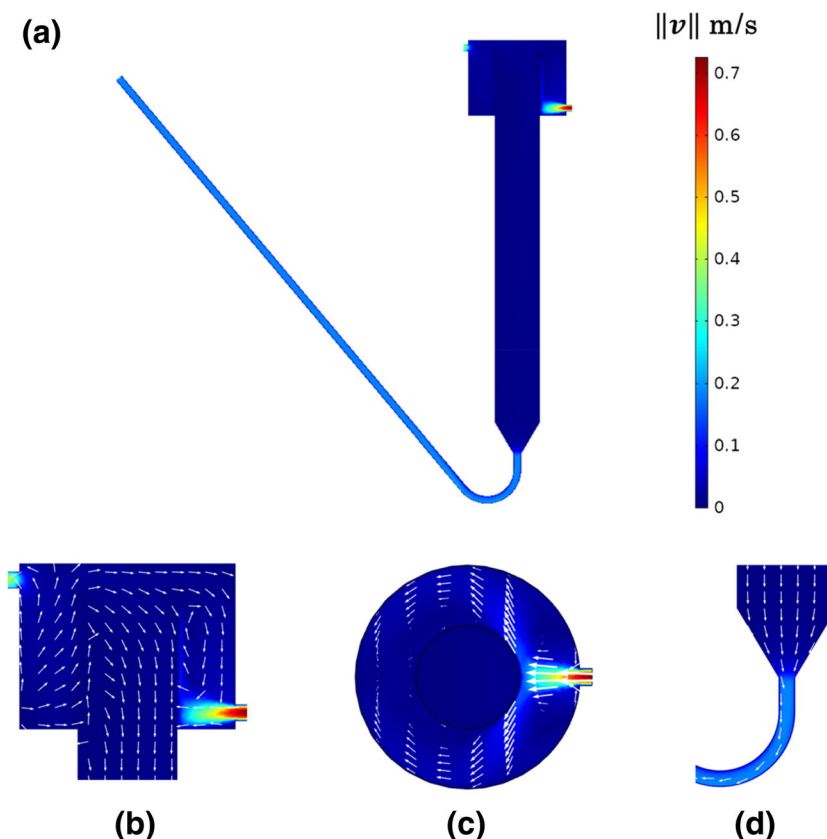
At the filament surface ($r = R$), constant concentrations are applied:

$$C_{\text{H}_2\text{O}}(R, t) = C_{\text{H}_2\text{O}}^{\partial\Omega}. \quad (9)$$

$$C_{\text{IL}}(R, t) = 0. \quad (10)$$

At the filament center ($r = 0$), a symmetry condition is considered:

FIGURE 3 (a) A color plot of the velocity magnitude in a 2-D longitudinal cut of the spin bath; zooms on the upper part in a longitudinal cut and in a cross section cut at the inlet level are shown respectively in (b) and (c); a zoom on the conical bottom part and the curved tube (d). In (b), (c) and (d), the velocity arrow field is superimposed on the velocity magnitude color plot [Color figure can be viewed at wileyonlinelibrary.com]



$$\frac{dC_i}{dr}(0, t) = 0. \quad (11)$$

The filament radius (15.8 μm) was divided into 50 elements using the predefined physics-controlled mesh generation option.

The simulation was done for a duration of 4 s with a time step of 0.01 s. The simulation results are depicted in Figure 4(a). This figure shows the normalized IL fraction (with respect to the initial IL concentration) in the filament cross section as a function of time. The reader can notice that at 1.6 s almost all the IL diffused in the coagulation bath.

As stated earlier, the time scale can be converted to a distance traveled by the filament inside the bath, by multiplying it with the filament take-up velocity. The resulting take-up velocity is therefore 19.1 m/min, and the 1.6 s corresponds then to a traveled distance of 0.51 m inside the coagulation bath.

To better illustrate the simulation results, the integrated IL fraction over the filament cross section as a function of the traveled distance in the bath is depicted in Figure 4(b). The reader can clearly see that when the filament travels 1 m in the spin bath, the IL content in the filament has already dropped to almost 7%. The distance from the top of the water surface to the jet exit is about 1.9 m, substantially longer than the required

distance of 1 m in this case, for the near-complete diffusion of the IL in the spin bath.

Overall, these experimental and simulation results show that this novel spinning bath design, with its specific water flow dynamics and long enough filament regeneration length is efficient for single filament spinning. With its low volume, it opens the room to fast and unexpensive spinning trials in IL-containing coagulation bath which are more representative of continuous process conditions.

3.3 | Spinning in IL/ H₂O mixtures

3.3.1 | Spinnability results as a function of the bath composition

The dope spinning results in IL/water mixtures were quite surprising and successful up to significant IL content in the bath. The details about spinnability are given in Figure S5 in the ESI.

In brief, dope spinning up to DR = 12 was successful with up to 30 wt% of IL in the spin bath. With 45 wt% of IL in the bath, we could surprisingly achieve a DR = 8, which is regarded as good considering the relatively high IL concentration in the coagulation mixture. Increasing the IL concentration further to 60 wt% resulted in a drop

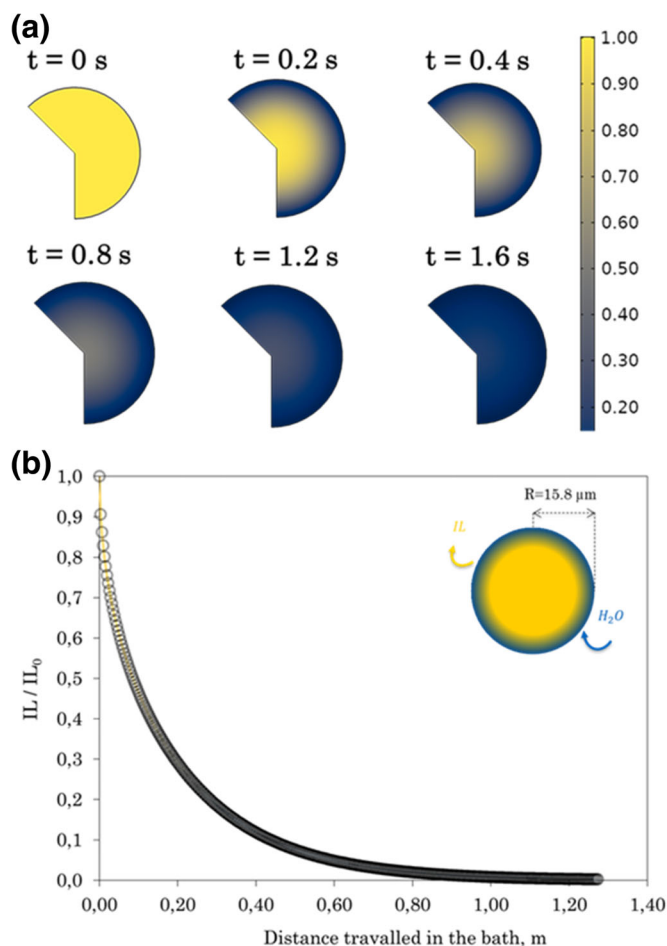


FIGURE 4 (a) Normalized IL fraction (with respect to the initial IL concentration) in the filament cross section as a function of time. The color bar refers to the IL fraction; (b) Integrated IL fraction over the filament cross section as a function of the traveled distance in the bath. Spinning conditions: DR = 10, $v_{\text{ext}} = 1.9$ m/min, bath temperature = 10°C . DRs, draw ratios; IL, ionic liquid [Color figure can be viewed at wileyonlinelibrary.com]

of the maximal achievable DR to 3. Although the DR is low, the result is still impressive regarding the high IL concentration in the bath. Beyond this DR, the spinning was not stable at all.

Referring to the literature, we could not find similar results on the spinnability of cellulose solution in IL using IL/water mixtures in the coagulation bath. In most of the studies, the cellulose regeneration and dope spinnability is reported in a pure water bath.²⁹

Those results have direct consequences the up-scaled continuous process. Indeed, the possibility to operate at a relatively high equilibrium concentration of IL in the spin bath implies an energy cost saving in the solvent recovery part, using for instance water evaporation to thermally separate water and IL.

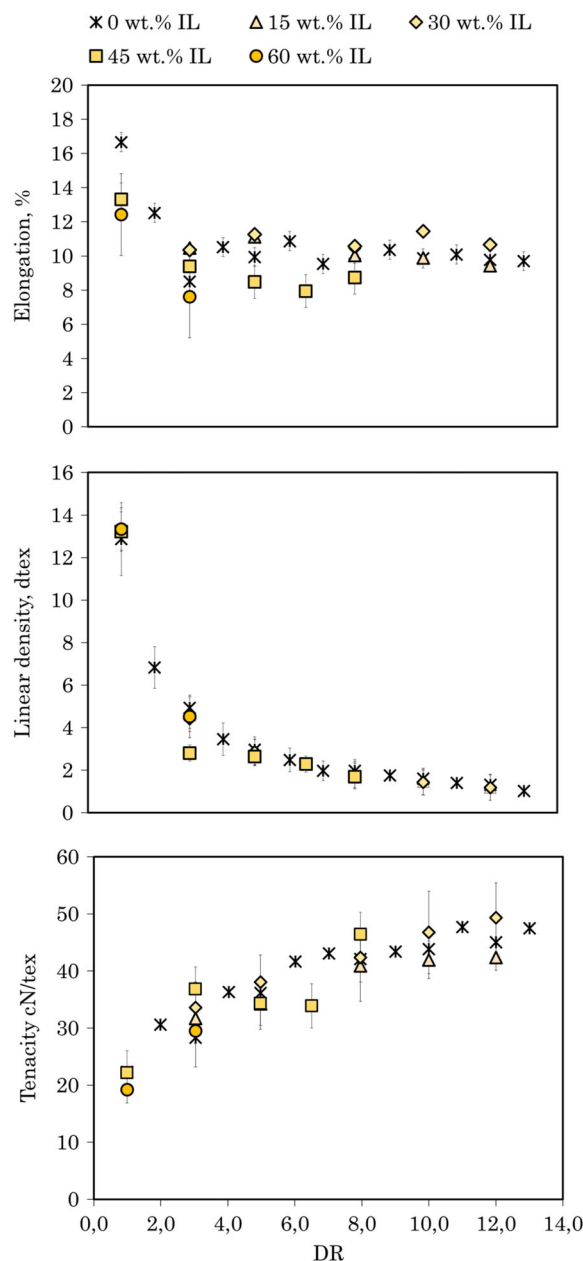


FIGURE 5 Fibers properties as a function of the DR for the different IL concentrations in the bath. Spinning conditions: $v_{\text{ext}} = 1.9$ m/min, bath temperature = 10 – 13°C . DRs, draw ratios; IL, ionic liquid [Color figure can be viewed at wileyonlinelibrary.com]

3.3.2 | Fiber properties as a function of the bath composition

Titer, tenacity and elongation

The fiber titer, tenacity and elongation as a function of the DR for the different IL concentrations in the bath are shown in Figure 5.

The fiber titer was not affected by the IL concentration in the bath, but only dependent on the DR. In the air gap, the titer or thickness of the spun filaments is reduced when applying a higher stretch on the spun filaments.

TABLE 1 Fibers crystallinity and crystal width values as a function of the DR and IL concentration in the spin bath

Experimental conditions		CI (%)		CW _{hkl} (Å)	
IL wt%	DR	9.0–50.0	err	average 3 peaks	err
0	3	35	0	33	0
	8	37	1	33	0
	12	37	1	33	0
15	3	35	3	32	0
	8	36	0	32	1
	12	37	0	32	0
30	3	36	1	32	1
	8	37	0	32	0
	12	36	3	32	0
45	3	37	0	33	1
	8	36	0	32	1
60	3	37	0	32	0

Abbreviations: DRs, draw ratios; IL, ionic liquid.

The tenacity of the fibers increases notably until DR 8 before leveling-off regardless of the IL concentration in the bath. By increasing the draw ratio, the cellulose chains are subjected to greater extensional stresses which enhance their alignment. The ordering of the molecules creates a packed network and cohesive forces between neighboring molecules are thus formed. The tenacity does not show any systematic variation with the IL concentration in the spin bath. The highest tenacity observed at DR = 8 corresponds to a fiber spun in a 45 wt%, while the tenacity values at the other concentrations were almost superimposed. Similarly, at DR = 12, the highest tenacity was observed for 30 wt% IL in the bath, while the lowest was observed at 15 wt% IL in the bath.

Between 0 and 30 wt% of IL in the bath, the fiber elongation is unaffected by the IL concentration. However, beyond 45 wt% of IL in the bath, the fiber elongation decreased in comparison to the values obtained in the range of 0–30 wt% IL in the bath. Those results suggest that going beyond 30 wt% of IL in the bath may be detrimental to the fiber elongation.

Overall, the results suggest that the presence of IL in the bath can have positive effects on the fiber tenacity development, but at the same time affects negatively the elongation for IL concentration in the bath exceeding 45 wt%. Those changes in the mechanical properties might be related to changes in the kinetics of the coagulation and regeneration steps, which rates would be directly affected by the amount of IL in the bath.^{3,7,12}

Crystalline structure of the spun fibers

Background corrected intensity profiles from 0, 15, 30, 45, and 60 IL concentration at DR 3 are shown in Figure S6 in the ESI. No shift was observed for the peak

position by different IL concentrations, indicating the identical cellulose II crystal structure for all the IL concentrations in the spin bath. [DBNH][OAc] molecules did not remain in the crystalline lattice of cellulose II after final washing of fibers in water.

The fibers crystallinity and crystal width values as a function of the DR and IL concentration in the spin bath are shown in Table 1. Crystal size was estimated to be approximately 32 Å for all the samples. As expected from the previous reports,²⁸ DR did not alter the crystallite dimension of cellulose II phase. Interestingly, the IL concentration in the bath did not affect the crystal width neither. Recent small angle X-ray scattering study showed the absence of crystallization up to 50 wt% IL concentration for the case of homogenous cellulose solution in [DBNH][OAc],¹² and therefore spinodal decomposition was proposed for the regeneration system of cellulose solution in [DBNH][OAc]. Our current study shows that the same size crystallites were recovered after the spinning in 0–60 wt% IL concentration in the spin bath and subsequent washing by water. Despite cations may bound to cellulose preventing crystallization of cellulose at high IL concentration, spinning was possible at low DR. This result indicates that the shear force during the spinneret extrusion and air gap already triggers the alignment and nucleation of cellulose chains, and such initial structure formation probably allows the spinning of the dope even under the high IL concentration in the spin bath. If the spinnability is assured by such an initial structure formation, the final crystallites dimension can be the same in spun fiber after final washing by water. In other word, the residual IL in the spun fiber during the spinning does not affect the crystalline dimension of cellulose II phase if the fibers were finally washed with water.

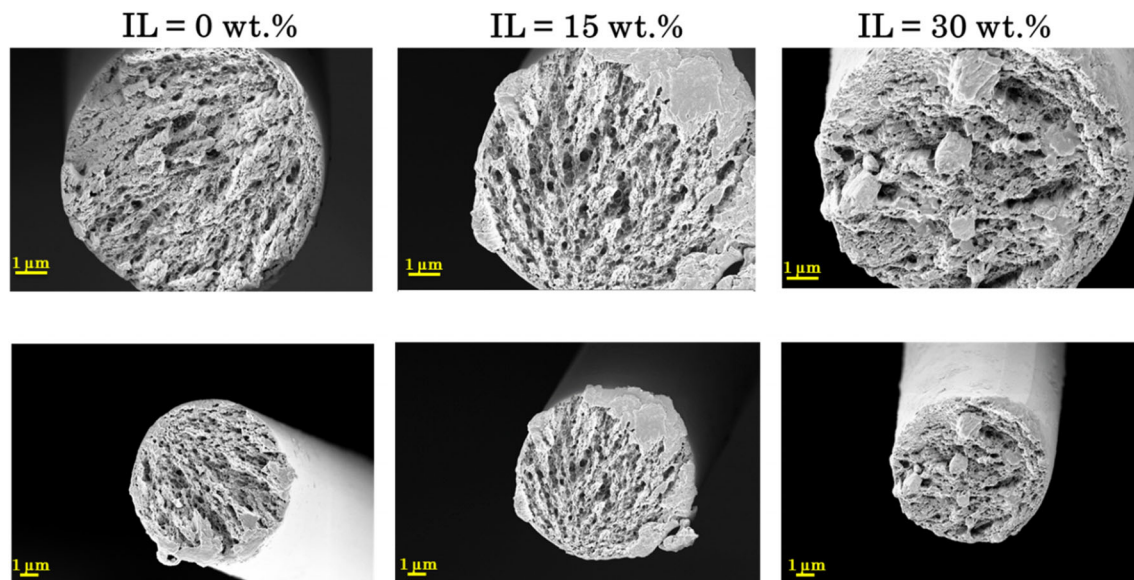


FIGURE 6 SEM images of fibers spun at DR 12 with 0 to 30 wt% of IL in the coagulation bath. DRs, draw ratios; IL, ionic liquid; SEM, scanning electron microscopy [Color figure can be viewed at wileyonlinelibrary.com]

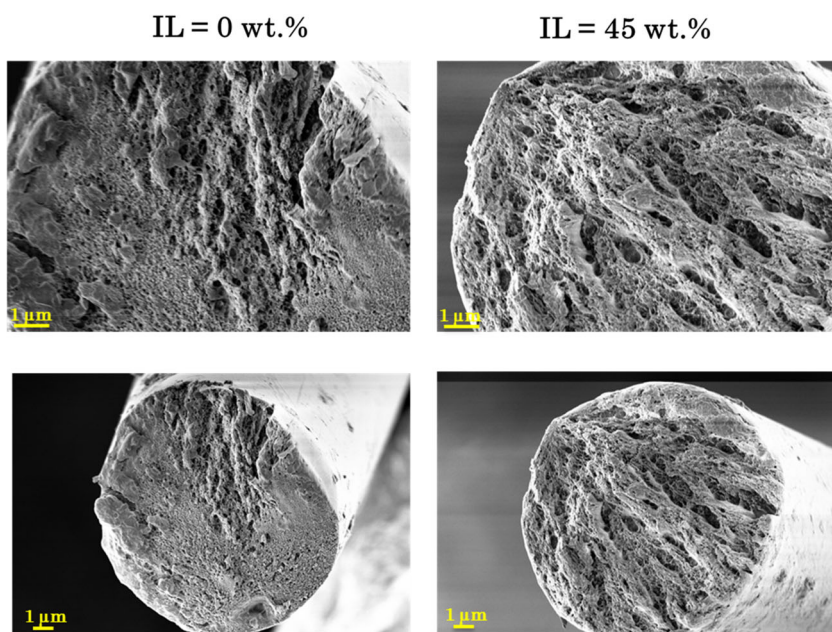


FIGURE 7 SEM images of fibers spun at DR 8 with 0 and 45 wt% IL in the coagulation bath. DRs, draw ratios; IL, ionic liquid; SEM, scanning electron microscopy [Color figure can be viewed at wileyonlinelibrary.com]

A few studies have reported the small increase of CI of Ioncell® fibers with respect to DR in the range over $DR = 2^{28,30}$. Our results were consistent with these studies for a pure water coagulation bath, and only small increase was observed for higher DR samples. Interestingly, slightly different trend was observed when the CI was obtained from higher IL concentration in the coagulation bath. Slightly greater CI was observed for higher IL wt% concentration only with $DR = 3$ fibers, but not with higher DR fibers. This result implies a little benefit for having certain amount of IL in spun fiber before the final

washing by water. However, these changes on CI were negligibly small, and no significant improvement was observed.

Overall, those results imply that precipitation kinetics, which vary with the IL concentration in the bath, do not have any significant effect on the final fibers crystalline properties.

Fiber morphology

The SEM images of the fibers spun at $DR = 12$ with 0 to 30 wt% of IL in the coagulation bath are shown in

Figure 6. The fiber morphology does not show major changes when increasing the IL concentration from 0 to 30 wt%, that is a smooth fiber surface, round cross-section, and homogeneous and dense fibrillary structure.¹ This observation still holds for an IL concentration of 45 wt% as shown in Figure 7, in which images of the fibers spun at DR = 8 in water and in 45 wt% IL coagulation bath are compared. As mentioned earlier, there is some evidence that the structure formation occurs via spinodal decomposition (diffusion controlled); this explains the relative homogeneous nanofibrillar structure along the cross-section.¹²

Although the fibrillar structure is observed for the different fibers at various IL concentrations in the bath, it seems to be a little bit more pronounced in the low-IL spin bath. Fibers spun into the spin bath with up to 30 or 45 wt% IL appear slightly less fibrillar and have a minor ductile character. This might be because the coagulation is not as fast as in the case of pure water, which gives the filament more time for relaxation.

Similar results were also reported in³¹ on the effect of NNMO concentration in the coagulation bath on the morphology of lyocell fibers. The authors found that the type of morphology of a regenerated cellulose object from a cellulose solution in NNMO-water is not very much dependent on the cellulose concentration or the bath composition, but strongly dependent on the state of the solution prior to regeneration (crystallized or molten).³¹

Liu et al. made also an attempt to correlate the coagulation rate of an $\text{NH}_3/\text{NH}_4\text{SCN}$ - Cellulose solution in various coagulation conditions, to the corresponding final fiber structure and fiber tensile properties; however, they could not find any correlation. The authors think that this may be due to the fact that the growth rate of the coagulated layer of spinning thread during the process of fiber formation, does not directly govern the composition of the coagulated layer which is believed to be a key factor affecting the fiber structure and consequently the fiber properties.¹⁰

Altogether, those results suggest that in a continuous process, spinning in 30 wt% IL solution would be perfectly possible and the spun fibers would have properties similar to those obtained in pure water.

4 | CONCLUSION AND PERSPECTIVES

A novel, small-volume vertically arranged spin bath was successfully developed for an air gap lyocell-type spinning process. A maximum regeneration bath length with a minimum free volume characterizes the concept of the

spin bath. The spin bath showed very good spinning performances of [DBNH][OAc]-cellulose dopes at high DRs and spinning duration, using a single filament. Those good spinning performances were achievable because of the high regeneration bath length combined to optimized flow hydrodynamics.

Using this new device, it was possible to get a step further in the optimization of the Ioncell[®] process and simulate a process closed loop operation by performing single filament spinning in IL/water mixtures. It came out from the experiments that spinning of [DBNH][OAc]-cellulose dopes in a coagulation bath containing up to 30 wt% of IL was possible without any major change in the dope spinnability or fibers mechanical and crystalline properties. At 45 wt% of IL in the spinning bath, spinning was still possible but at a lower DR and resulting in lower quality fibers.

Those results have direct consequences on an up-scaled continuous process, as the possibility to spin in relatively concentrated bath implies lower solvent recycling costs using for instance thermal separation of IL and water.

ORCID

Chamseddine Guizani  <https://orcid.org/0000-0001-7652-2751>

REFERENCES

- [1] A. Michud, M. Tanttu, S. Asaadi, Y. Ma, E. Netti, P. Kääriäinen, A. Persson, A. Berntsson, M. Hummel, H. Sixta, *Text. Res. J.* **2016**, 86, 543.
- [2] Michud, A.; King, A.; Parviainen, A.; Sixta, H.; Hauru, L.; Hummel, M.; Kilpeläinen, I. **2016**.
- [3] L. K. J. Hauru, M. Hummel, K. Nieminen, A. Michud, H. Sixta, *Soft Matter*. **2016**, 12, 1487.
- [4] S. Asaadi, M. Hummel, S. Hellsten, T. Härkäsalmi, Y. Ma, A. Michud, H. Sixta, *ChemSusChem* **2016**, 9, 3250.
- [5] Y. Ma, M. Hummel, I. Kontro, H. Sixta, *Green Chem.* **2018**, 20, 160.
- [6] C. Olsson, G. Westman, *J. Appl. Polym. Sci.* **2013**, 127, 4542.
- [7] A. Hedlund, T. Köhnke, H. Theliander, *Macromolecules* **2017**, 50, 8707.
- [8] C. A. Hall, K. A. Le, C. Rudaz, A. Radhi, C. S. Lovell, R. A. Damion, T. Budtova, M. E. Ries, *J. Phys. Chem. B* **2012**, 116, 12810.
- [9] G. Jiang, W. Huang, T. Zhu, C. Zhang, A. K. Kumi, Y. Zhang, H. Wang, L. Hu, *Cellulose* **2011**, 18, 921.
- [10] C. -k. Liu, J. A. Cuculo, B. Smith, *J. Polym. Sci. Part B Polym. Phys.* **1989**, 27, 2493.
- [11] O. Biganska, P. Navard, *Biomacromolecules* **2005**, 6, 1948.
- [12] Y. Nishiyama, S. Asaadi, P. Ahvenainen, H. Sixta, *Cellulose* **2019**, 26, 281.
- [13] A. Hedlund, T. Köhnke, H. Theliander, *Nord. Pulp Pap. Res. J.* **2015**, 30, 32.
- [14] A. Hedlund, T. Köhnke, J. Hagman, U. Olsson, H. Theliander, *Cellulose* **2019**, 26, 1545.

- [15] A. Hedlund, H. Theliander, T. Köhnke, *Cellulose* **2019**, 26, 8525.
- [16] Y. Ma, J. Stubb, I. Kontro, K. Nieminen, M. Hummel, H. Sixta, *Carbohydr. Polym.* **2018**, 179, 145.
- [17] L. K. J. Hauru, M. Hummel, A. Michud, H. Sixta, *Cellulose* **2014**, 21, 4471.
- [18] L. K. J. Hauru, M. Hummel, A. Michud, H. Sixta, *Cellulose* **2017**, 24, 3109.
- [19] V. Klar, H. Orelma, H. Rautkoski, P. Kuosmanen, A. Harlin, *ACS Omega* **2018**, 3, 10918.
- [20] Hedlund, A. Air gap spinning of cellulose fibers from ionic solvents, **2013**.
- [21] A. Michud, M. Hummel, H. Sixta, *J. Appl. Polym. Sci.* **2016**, 133, 1.
- [22] A. Savitzky, J. . G. Marcel, *Anal. Chem.* **1964**, 36, 1627.
- [23] S. Brückner, *J. Appl. Crystallogr.* **2000**, 33, 977.
- [24] K. Frost, D. Kaminski, G. Kirwan, E. Lascaris, R. Shanks, *Carbohydr. Polym.* **2009**, 78, 543.
- [25] Newville, M., Stensitzki, T., Allen, D. B., M. Rawlik, A. Ingargiola, A. Nelson, *LMFIT: Non-Linear Least-Square Minimization And Curve-Fitting For Python* **2016**. <https://ui.adsabs.harvard.edu/abs/2016ascl.soft06014N>.
- [26] G. Ashiotis, A. Deschildre, Z. Nawaz, J. P. Wright, D. Karkoulis, F. E. Picca, J. Kieffer, *J. Appl. Crystallogr.* **2015**, 48, 510.
- [27] N. Yoshiharu, K. Shigenori, W. Masahisa, O. Takeshi, *Macromolecules* **1997**, 30, 6395.
- [28] S. Asaadi, M. Hummel, P. Ahvenainen, M. Gubitosi, U. Olsson, H. Sixta, *Carbohydr. Polym.* **2018**, 181, 893.
- [29] F. Hermanutz, M. P. Vocht, N. Panzier, M. R. Buchmeiser, *Macromol. Mater. Eng.* **2019**, 304, 1.
- [30] H. Sixta, A. Michud, L. Hauru, S. Asaadi, Y. Ma, A. W. T. King, I. Kilpeläinen, M. Hummel, *Nord. Pulp Pap. Res. J.* **2015**, 30, 43.
- [31] O. Biganska, P. Navard, *Cellulose* **2009**, 16, 179.

SUPPORTING INFORMATION

Additional supporting information may be found online in the Supporting Information section at the end of this article.

How to cite this article: Guizani C, Larkiala S, Moriam K, et al. Air gap spinning of a cellulose solution in [DBNH][OAc] ionic liquid with a novel vertically arranged spinning bath to simulate a closed loop operation in the Ioncell[®] process. *J Appl Polym Sci.* 2021;138:e49787. <https://doi.org/10.1002/app.49787>